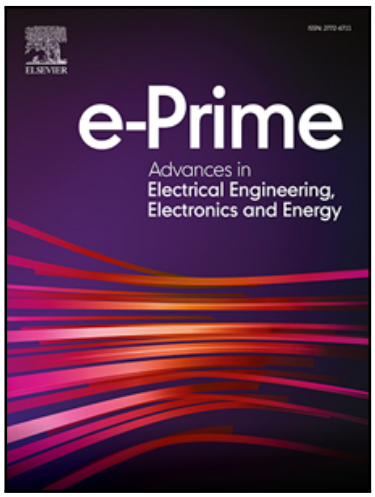

Current balancing of scalar-controlled induction motors with long imbalanced cables for artificial lift systems

Georgios I. Orfanoudakis , Michael A. Yuratich ,
Suleiman M. Sharkh

PII: S2772-6711(23)00286-3
DOI: https://doi.org/10.1016/j.prime.2023.100391
Reference: PRIME 100391

To appear in: *e-Prime - Advances in Electrical Engineering, Electronics and Energy*

Received date: 22 August 2023
Revised date: 11 November 2023
Accepted date: 7 December 2023

Please cite this article as: Georgios I. Orfanoudakis , Michael A. Yuratich , Suleiman M. Sharkh , Current balancing of scalar-controlled induction motors with long imbalanced cables for artificial lift systems, *e-Prime - Advances in Electrical Engineering, Electronics and Energy* (2023), doi: https://doi.org/10.1016/j.prime.2023.100391

Highlights

- Current balancing of induction motors driven by scalar-controlled variable speed drives.
- Based on Second-Order Generalized Integrators (SOGIs) and Synchronous Reference Frame (SRF) current control.
- No need for additional hardware, position sensor or observer.
- Simple, robust, computationally effective implementation, independent of the cable characteristics.

http://dx.doi.org/10.1016/j.ijepes.2021.000000

Current balancing of scalar-controlled induction motors with long imbalanced cables for artificial lift systems

Georgios I. Orfanoudakis[a], Michael A. Yuratich[b], Suleiman M. Sharkh[c,*]

[a]*Electrical and Computer Engineering department, Hellenic Mediterranean University (HMU), Heraklion, Crete, Greece, 71410*
[b]*TSL Technology Ltd, Ropley, SO24 0BG, UK*
[c]*Mechatronics Research Group, Mechanical Engineering, Faculty of Engineering and Physical Sciences, University of Southampton, SO17 1BJ, UK*

Abstract

Induction motor current imbalance increases losses, torque ripple and vibrations. Current imbalance is known to appear in artificial lift systems, where motors are driven over long imbalanced cables. Power hardware modifications, namely transposition of cable phases in the wellbore, adjustment of the step-up transformer taps, and addition of balancing inductors have so far been proposed to suppress the imbalance. However, these solutions compromise the system's reliability or involve costly additional equipment, which must be customized according to the cable characteristics. This paper proposes a control method for current balancing of induction motors driven by scalar-controlled variable speed drives. In the proposed method, Second-Order Generalized Integrators (SOGIs) are used to extract the negative-sequence component of the motor currents, which is then suppressed by a Synchronous Reference Frame (SRF) current controller. The frequency and angle information required by the SOGIs and the SRF controller are obtained directly from the scalar algorithm, without needing a position sensor or observer, thus offering a novel, simple, robust and computationally effective implementation, which is also independent of the cable characteristics. The paper presents MATLAB/Simulink simulation results to illustrate the method's operating principles and performance in a variety of transient conditions. Experimental results obtained using full-scale equipment are also provided to demonstrate its effectiveness.

Keywords: Current balancing; Second-Order Generalized Integrator (SOGI); V/f control; Scalar control; Current imbalance; Artificial lift; Electric Submersible Pump (ESP)

Nomenclature

ESP	Electric Submersible Pump
IM	Induction Motor
PLL	Phase-Locked Loop
(D)SOGI	(Dual) Second-Order Generalised Integrator
SRF	Synchronous Reference Frame
VSD	Variable Speed Drive

* Corresponding author. Tel.: +44 23 8059 5000
E-mail address: s.m.sharkh@soton.ac.uk
http://dx.doi.org/10.1016/j.ijepes.2021.00.000
0142-0615 /

1. Introduction

Induction motor (IM) current imbalance increases power losses, which lead to inefficiency and overheating while also generating torque ripple and vibrations. Depending on the degree of imbalance, a motor may need to be derated by up to 25% to avoid these effects [1 – 3]. Current imbalance can be caused by an imbalance of the mains voltages in line-connected motors. It is generally not observed in motors supplied by variable-speed drives (VSDs), which normally can generate balanced output voltages under all allowed supply conditions. However, in certain applications such as artificial lift for oil/water pumping using Electrical Submersible Pumps (ESPs), current imbalance can be introduced due to the imbalanced impedance of the connecting cable, which can be several kilometers long. The widely used flat steel-armored cables, with a typical cross-section as shown in Fig. 1, exhibit significantly imbalanced phase inductances [4, 5].

The common method for suppressing the resulting current imbalance is to divide the cable into three portions of equal length, transpose its conductors and rejoin (splice) them, so that each phase current flows equally through the middle and the outer conductors. However, cable splices are known points of failures that should ideally be avoided [6, 7]. With this aim, the addition of balancing inductors and the adjustment of step-up transformer taps have been proposed as alternative approaches for current balancing [7 – 9]. The main drawbacks of these approaches are that they require knowledge/measurement of the cable imbalance characteristics (i.e., self/mutual inductance matrix) and custom-designed power hardware, which adds to the system's cost.

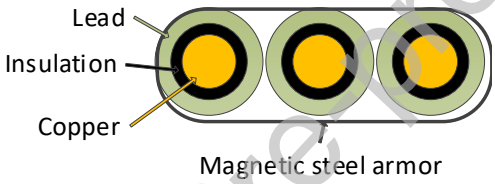

Fig. 1. Cross-section of an ESP flat steel armored cable.

Control methods for current balancing have been proposed for three-phase inverters connected to imbalanced grids [10 – 12] and vector-controlled VSDs for permanent magnet synchronous [13 – 15] and induction motors [16, 17]. Current balancing is typically achieved by the addition of a negative-sequence current suppression feedback control loop, extracting the symmetrical components of the current and suppressing the negative-sequence components using PI controllers operating in the Synchronous Reference Frame (SRF) [10 – 20]. Most of the above methods require an angle and/or a frequency input. In grid-connected inverters, this is the angle of the voltage at the Point of Common Coupling (PCC), normally estimated by a Phase Locked Loop (PLL), while in vector-controlled VSDs, it is the electrical angle of the magnetic field of the rotor, measured using a suitable sensor or estimated by an observer. Due to cost and reliability reasons, observers are normally preferred over position sensors in applications requiring motor speed (not position) control, while they are the only option for artificial lift systems, because of the long distance between the VSD and the motor. On the other hand, the performance of observers can be affected by non-idealities in the system and/or voltage-current measurements, such as imbalances, harmonics, and DC offsets. Even modern observers, such as those based on Second-Order Generalized Integrators (SOGIs) [21], are affected by the above disturbances. This is because a SOGI-PLL typically consists of a) a SOGI/DSOGI that acts as a filter around the fundamental frequency, and b) a classical Synchronous Reference Frame (SRF) PLL, which is very sensitive to these disturbances. Given that the SOGI/DSOGI is not an ideal band-pass filter (while DC offsets are not filtered in the quadrature SOGI outputs at all), the output of the SOGI/DSOGI passed to the SRF PLL is not free from DC offset / harmonics, thus degrading the angle-frequency estimation by the PLL. Consequently, the basic SOGI-PLL structure must be extended to accommodate advanced features that offer immunity to disturbances [22 – 27]. However, this significantly increases the computational complexity of vector control algorithms and can compromise their dynamic response. The impact is even higher for scalar (constant V/f) IM control algorithms, in which observers are not typically included at all, since they are not required. This renders the abovementioned current balancing methods practically inapplicable to the widely used scalar algorithms for IMs.

This paper proposes a current balancing control method for scalar-controlled IM VSDs. The method employs SOGI-based structures and SRF current controllers in a novel manner, which is suited to scalar IM control. The key characteristic of the proposed method is that it does not require a sensor or observer providing angle/frequency information; instead, it uses the angle and frequency values that scalar algorithms generate internally to produce their balanced voltage references. Moreover, the method does not require knowledge of cable parameters and relevant calculations, or modifications to the power equipment, which form the basis for other current balancing approaches. As a result, it presents the following advantages:

- It is simple to implement and computationally efficient.
- It does not need to be adapted based on the imbalanced cable parameters.
- It does not incur any costs associated with new/modified power equipment or position/speed sensors.
- It is more robust than sensor-based methods, as it does not rely on their performance and health of sensor-drive connections.
- It is more robust than position observer-based methods, as it uses an internally-generated angle which is immune to disturbances such as imbalances, harmonics and DC offsets.
- It can be readily incorporated as an add-on to existing scalar control algorithms.

The paper is structured as follows. Section 2 contains a description of the proposed current balancing method. Section 3 includes detailed simulation results and Section 4 presents experimental results. A discussion follows in Section 5, while Section 6 concludes the paper.

2. Proposed method

2.1. Scalar control voltage references

Scalar VSDs generate balanced voltages with a pre-determined ratio between amplitude and frequency (with an amplitude boost at low frequencies), in accordance with the motor nameplate. Namely, at any given time, a scalar control algorithm generates three voltage references, $u_{abc,sc}$ (subscript "sc" stands for "scalar"):

$$u_{abc,sc}(t) = \hat{V}_{sc}\,(t)\,\sin(\theta_{sc}(t) + \theta_{abc}) \tag{1}$$

where $\hat{V}_{sc}$ is the demanded peak phase voltage normalized to half of the DC-link voltage and θ_{abc} is equal to 0, −120 and +120 degrees for the three phases, respectively. The angle θ_{sc} is calculated as

$$\theta_{sc}(t) = \int \omega_{sc}(t)\mathrm{d}t \tag{2}$$

where ω_{sc} is the electrical angular frequency that corresponds to the demanded electrical frequency f_{sc}:

$$\omega_{sc} = 2\pi f_{sc}\ . \tag{3}$$

2.2. Proposed Control Structure

Conventional scalar control methods always generate a balanced set of three-phase voltages. For imbalanced loads, however, the voltages need to be appropriately imbalanced, in order to balance the currents. Fig. 2 presents an overall block diagram of the proposed current balancing method.

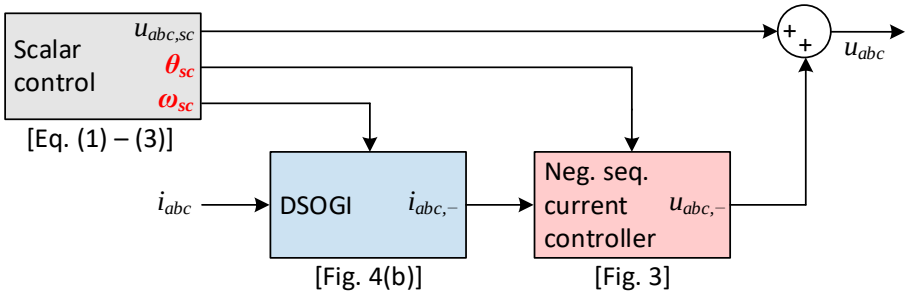

Fig. 2. Proposed SOGI-based current balancing method for scalar-controlled IMs.

In addition to the scalar controller based on equations (1) – (3), a negative sequence current suppression controller (Fig. 3) is used to add a negative-sequence component, $u_{abs,-}$, to $u_{abc,sc}$ to generate the PWM reference voltage, u_{abc}. The negative-sequence current component is estimated using a simplified dual second-order generalized integrator (DSOGI), which is based upon the SOGI and SOGI-QSG (QSG: Quadrature Signal Generator) structures [21], shown in Fig. 4 (a). The SOGI-QSG has been used in the literature to address filtering, integration, synchronization, and imbalance issues in grid-connected converters [18 – 27] and motor drives [28 – 37]. With reference to imbalance, two SOGI-QSGs operating in the alpha-beta coordinates are used as illustrated in Fig. 4(b) to form a DSOGI structure [18]. If the angular frequency ω' provided to a DSOGI is the fundamental frequency of its three-phase input signals, i_{abc}, a DSOGI can extract its positive- and negative-sequence components, band-pass filtered around ω'. In the literature, DSOGIs have primarily been applied on imbalanced voltage signals, with the aim of extracting their positive-sequence component [10, 13, 18, 20, 29]. The positive-sequence component is a balanced set of three-phase voltages, thus the DSOGI is used in this case as an imbalance filter. Its balanced outputs are supplied to common PLLs and observers, preventing distortions that appear on their estimated angle and frequency when they operate on imbalanced signals. In the proposed method, the input signals of the DSOGI are currents, i_{abc}, while the DSOGI is simplified as compared to [18, 19] to extract only the negative-sequence current component, $i'_{abc,-}$, thus saving computational resources.

The amplitude of $i'_{abc,-}$ is proportional to the degree of the imbalance between the three input currents. To suppress the current imbalance, the negative-sequence PI controllers are given zero reference values, as shown in Fig. 2. This results in the generation of voltage references $u_{abc,-}$ which suppress the negative-sequence component of i_{abc} and thus the imbalance. These reference voltages are added to the normal (balanced) reference voltages $u_{abc,sc}$, to form the actual references u_{abc}, as shown in Fig. 2.

The tuning of the negative-sequence current PI controllers can be based on conventional methods for tuning (positive-sequence) current PI controllers for indirect vector control of induction motors [38]. Nevertheless, by means of simulations and experiments, it was also confirmed that the controller gains can be reduced significantly, while still achieving current balancing during steady-state operation. Lower gains can be preferable, for example, in order to avoid intense variations to the voltage references u_{abc}, which could cause over-modulation or resonance in VSDs with sine filters. Indicative values for the proportional gain and integral time constant are given in Section 3 for a 460 V – 50 HP induction motor.

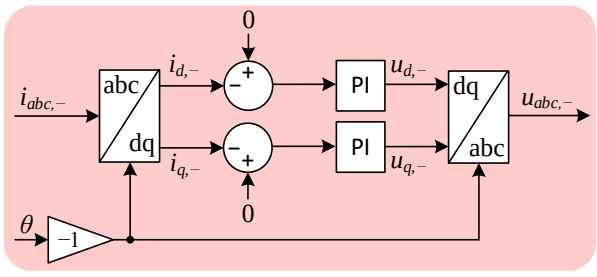

Fig. 3. Negative-sequence current controller.

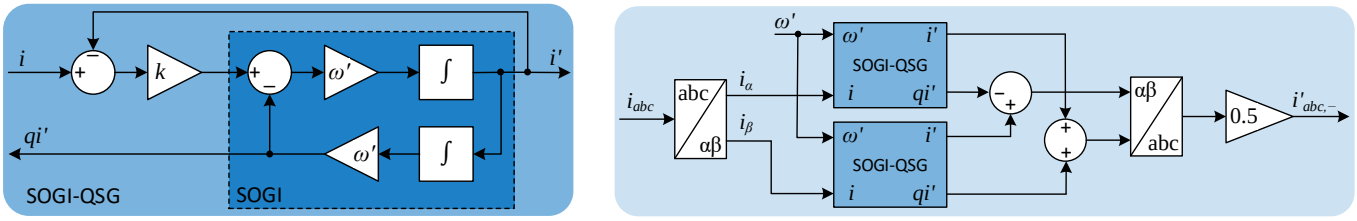

(a) (b)

Fig. 4. (a) SOGI and SOGI-QSG [21], (b) DSOGI with negative-sequence output [18].

2.3. Substitution of observer estimates by scalar control variables

Past-proposed current balancing approaches for grid-connected inverters and vector-controlled motor drives rely on the acquisition or estimation of frequency and angle information. With regards to motor control, the DSOGIs used to generate the symmetrical components of the currents require knowledge of the electrical angular frequency of the rotor magnetic field, ω_e, to be passed in as ω' in Fig. 4. Moreover, the electrical angle of the magnetic field of the rotor, θ_e, is required by the Park (abc-dq) and inverse Park (dq-abc) transformations of the SRF negative-sequence current controllers, to be passed in as θ in Fig. 3. In the case of ESP and other remote motor drive applications, both quantities are typically estimated by a flux observer, which must be designed/adapted to operate under imbalanced conditions [13]. However, such observers are not required by scalar control algorithms, and the implementation of a suitable observer would increase the computational burden and complexity of the control system.

The proposed approach avoids the need for observer implementation, by substituting ω_e and θ_e by appropriate quantities. Namely, as illustrated in Fig. 2, the angular frequency ω_{sc}, from (3), is used instead of ω_e, while the angle θ_{sc}, from (2), is used in place of θ_e. The DSOGI of Fig. 4 is therefore supplied with $\omega' = \omega_{sc}$ to extract the negative-sequence motor currents $i_{abc,-}$ from the measured motor currents, i_{abc}, while the transformations of the negative-sequence current controller in Fig. 3 are supplied with $\theta = \theta_{sc}$. Current balancing is achieved by the proposed method, because in steady-state conditions:

a) The scalar algorithm electrical angular frequency is equal to the angular frequency of the rotor magnetic field, i.e., $\omega_{sc} = \omega_e$. This is because in an induction machine, the stator and rotor magnetic fields always rotate synchronously under steady-state conditions [39]. Thus, a DSOGI supplied with ω_{sc} (the stator magnetic field electrical angular frequency) produces the same outputs as if it is supplied by ω_e (the rotor magnetic field electrical angular frequency).

b) Since ω_{sc} and ω_e are equal under steady state conditions, the difference between their integrals, that is, angles θ_{sc} and θ_e, is a constant. This relates to the fundamental condition for steady-state constant torque production, according to which, the magnetic fields of the stator and the rotor are displaced by a certain phase angle. The use of θ_{sc} instead of θ_e alters the values of the dq current components, $i_{d,-}$ and $i_{q,-}$ in Fig. 3. Namely, the constant difference between θ_{sc} and θ_e translates into an angle shift in polar coordinates. This retains the magnitude of the negative-sequence current component, but changes the ratio between $i_{d,-}$ and $i_{q,-}$. Nevertheless, the key point is that, because the references of the negative-sequence PI controllers in Fig. 3 are set to zero, both $i_{d,-}$ and $i_{q,-}$ are suppressed, irrespective of their actual values.

3. Simulation results

The MATLAB/Simulink simulation results presented in this section refer to the scalar control of an IM over an imbalanced cable, by a standard VSD equipped with a sine filter, using the proposed current balancing method. The induction motor nameplate and equivalent circuit parameters are listed in Tables 1 and 2, respectively. The cable connecting the VSD to the motor is assumed to be a 1400 m flat armoured submersible pump cable of size 4 AWG, which was estimated to have balanced resistances of 1.2 Ω per phase and imbalanced inductances equal to 1.5 mH for

the two outer conductors and 0.5 mH for the middle one. With regards to control parameters, the *k* gain for the SOGIs was set to 1, resulting in a damping ratio of 0.5 and a settling time of 25 ms [21]. The negative-sequence current PI controllers' proportional gain and integral time constant were set to 0.25 (V/A) and 20 ms, respectively, to achieve an overdamped response, with a settling time of about 1 s. This helps to meet an application requirement of low actuator torque with the aim of reducing mechanical stresses, while also improving the stability of the control system by decoupling the (fast) SOGI control loops from the negative-sequence current control loop.

Fig. 5(a) illustrates the effect of enabling the proposed current balancing method while the motor is running at its rated frequency and with a load of 100 Nm, which corresponds to half of its rated torque. The figure presents the drive output voltages, which are initially balanced, and the motor currents, which are imbalanced. The degree of imbalance, calculated according to the VUF definition [3, 40], is around 7.5%, as shown in the bottom-right graph. The electromagnetic motor torque, which exhibits significant ripple due to the imbalance, is shown in the bottom-left graph. At t = 5 s, current balancing is enabled. From this point onwards, the employed current controller injects a non-zero negative-sequence component into the inverter voltage references. As a result, the amplitude of the negative-sequence currents and the measured imbalance reduce to virtually zero at t = 6 s, while the torque ripple is suppressed. Figs. 5(b)-(c) include magnified plots to compare the waveforms of drive voltages-currents and motor torque before and after enabling current balancing. In practice, current balancing will normally be enabled throughout motor operation, thus the waveforms of Fig. 5(c) represent the steady-state behaviour.

Table 1. Motor nameplate parameters.

Parameter	Value
Voltage	460 V
Frequency	60 Hz
Speed	1780 rpm
Torque	200 Nm
Mech. power	50 HP

Table 2. Motor equivalent circuit parameters.

Parameter	Value
Stator resistance	99.61 mΩ
Stator leakage ind.	0.867 mH
Rotor resistance (Rr′)	58.37 mΩ
Rotor leakage ind. (Lr′)	0.867 mH
Magnetizing inductance	30.39 mH

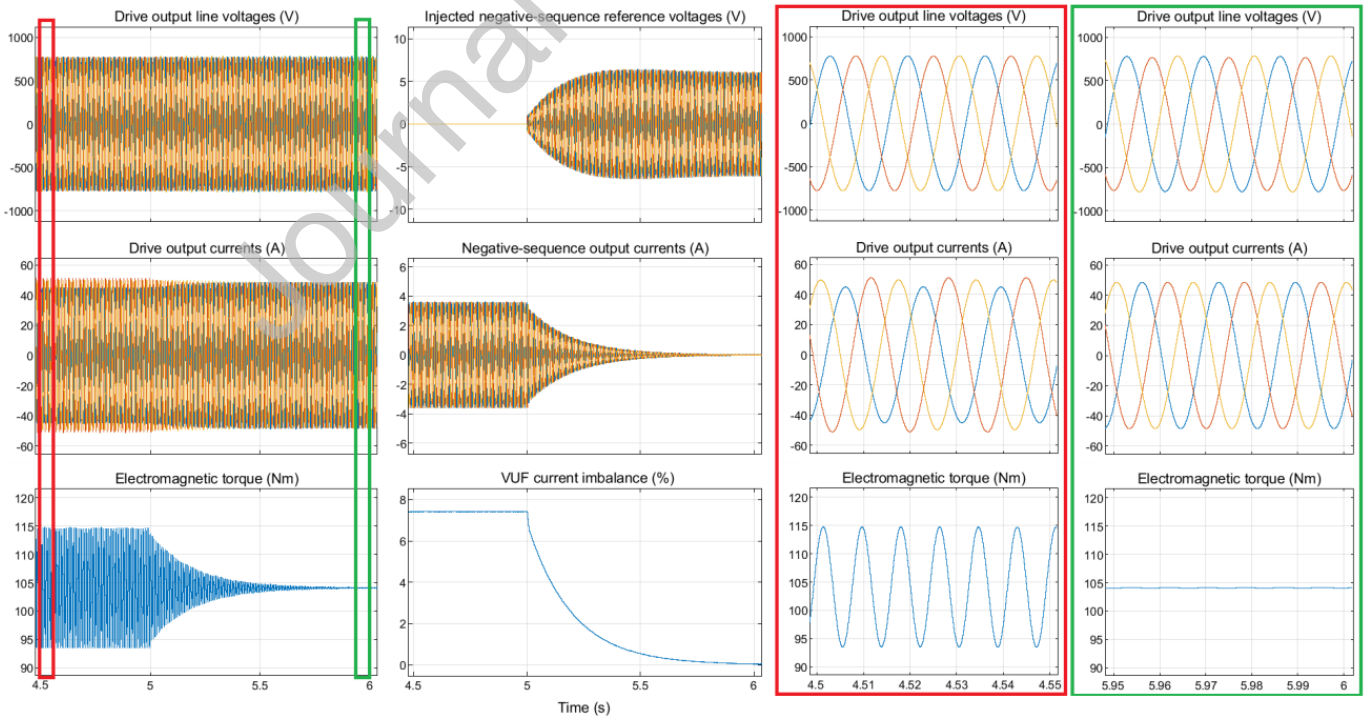

Fig. 5. Simulation results illustrating the effect of applying the proposed current balancing method, at t = 5 s. The graphs present (a) drive output voltages and currents, motor electromagnetic torque, injected negative-sequence inverter reference voltages, calculated negative-sequence currents

and percent imbalance, and magnified extracts of drive output voltages and currents, and motor electromagnetic torque, (b) before, and (c) after enabling current balancing.

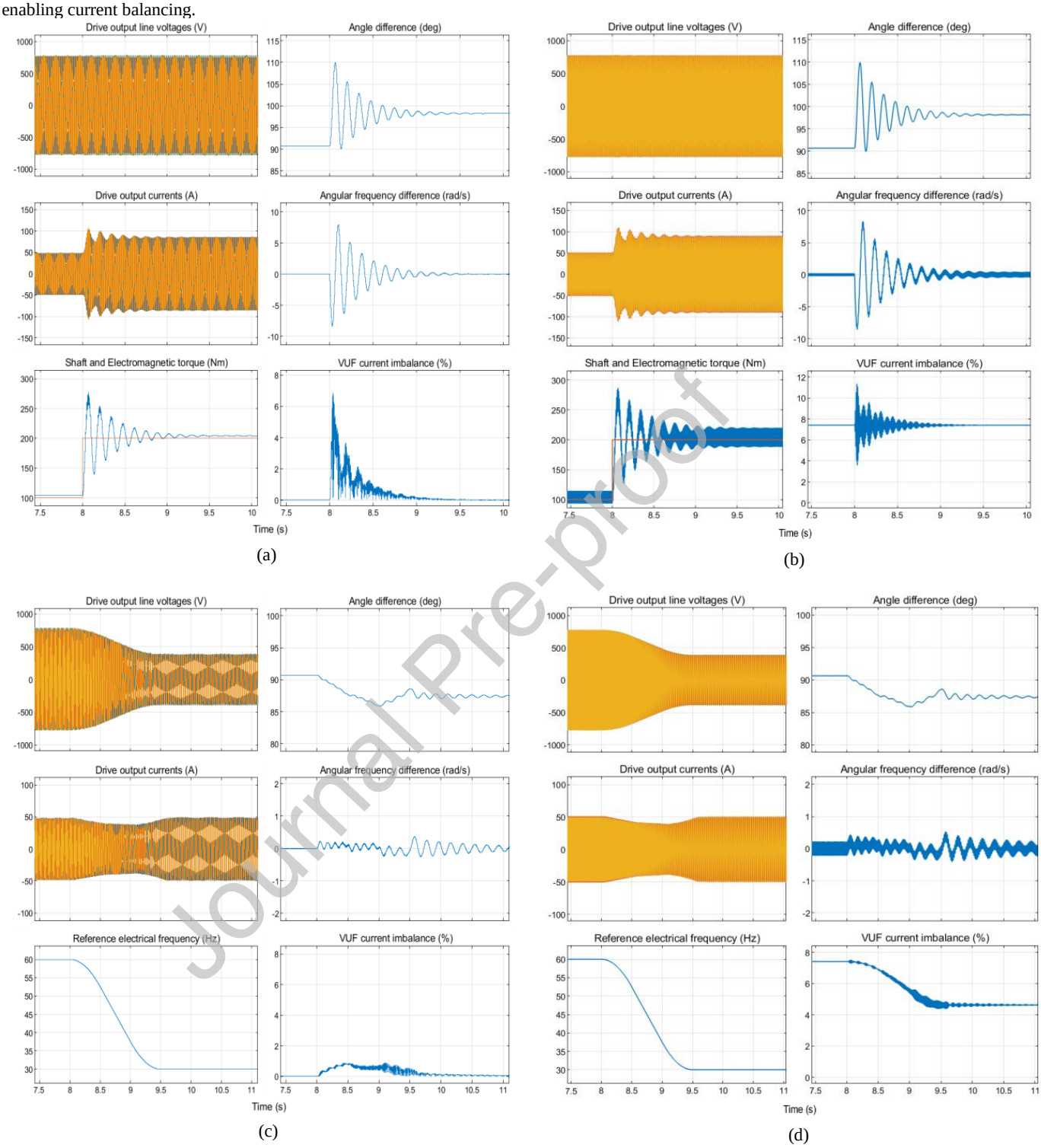

Fig. 6. Simulation results illustrating the response of the current balancing method to (a) a shaft torque step, from 100 Nm to 200 Nm, at t = 8 s, and (c) a reference frequency reduction, from 60 Hz to 30 Hz, within 1 s, starting at t = 8 s. For comparison, (b) and (d) present the respective responses with the method disabled. Each set of graphs presents the drive output voltages and currents, torque/frequency, angle θ_{sc} and angular frequency ω_{sc} difference from θ_e and ω_e, respectively, and percent imbalance.

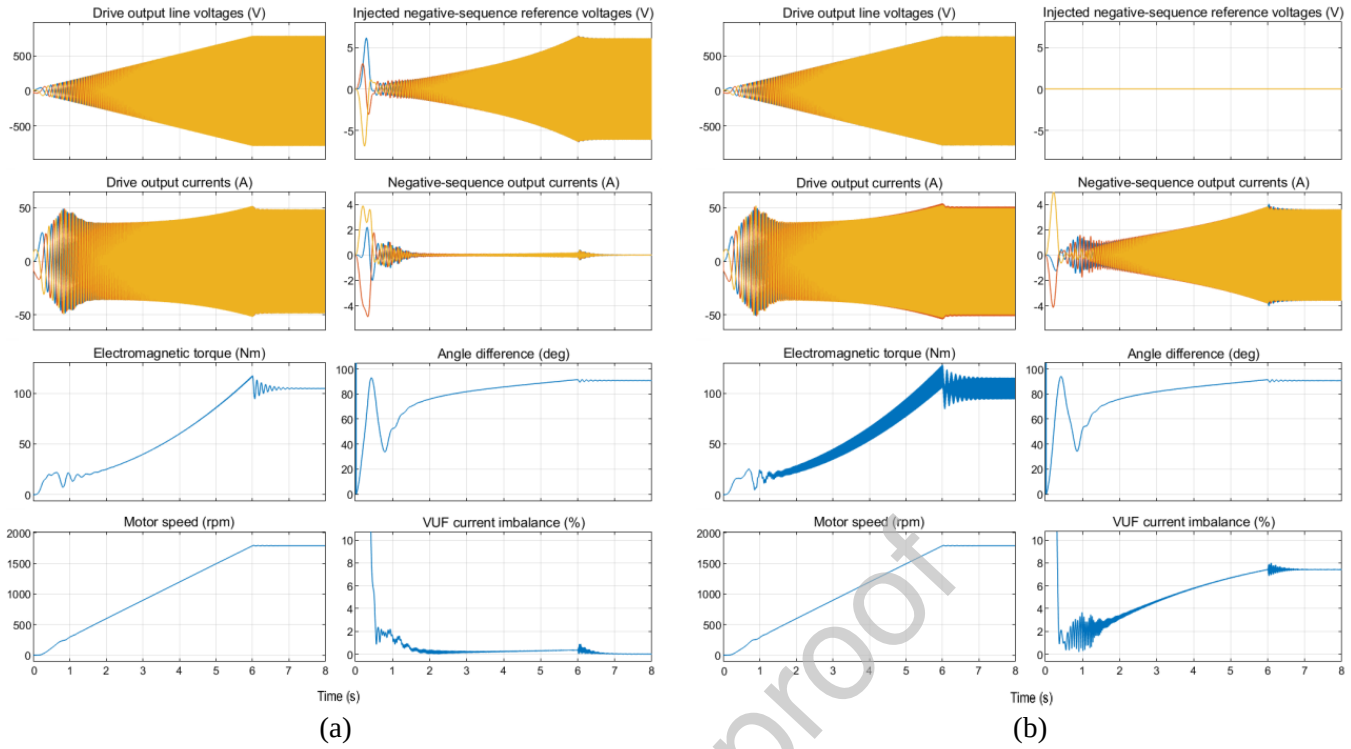

Fig. 7. Simulation results illustrating motor starting with the current balancing method (a) enabled, and (b) disabled. Each set of graphs presents the drive output voltages and currents, electromagnetic torque (quadratic), motor speed, injected negative-sequence inverter reference voltages, calculated negative-sequence currents, angle θ_{sc} difference from θ_e, and percent imbalance.

The results in Fig. 6(a, c) present the transient response of the (enabled) proposed method following (a) a torque step, and (c) a frequency change. They also demonstrate the relationships between angles θ_{sc} and θ_e, and angular frequencies ω_{sc} and ω_e, highlighted in the previous section. In Fig. 6(a), a shaft torque step from 100 to 200 Nm is applied at t = 8 s. It can be observed that the percent imbalance temporarily rises and drops to zero again when the new torque steady state is reached, at $t \approx 10$ s. The angular frequency difference ($\omega_e - \omega_{sc}$) is equal to zero at t = 8 s and returns to zero at $t \approx 10$ s. Moreover, the angle difference ($\theta_e - \theta_{sc}$) has a constant value before t = 8 s and acquires a new value during the transient, which remains constant after the transient elapses. Similar effects can be seen in Fig. 6(c), which presents the response to a reference frequency drop from 60 to 30 Hz, within 1.5 s. The above two observations confirm the principles for the formulation of the proposed method. Furthermore, the oscillations on the torque, angle and angular frequency waveforms in Figs. 6(a, c) are inherent to the scalar control algorithm and are not caused by the current balancing algorithm. This is confirmed by the comparative simulation results presented in Figs. 6(b, d), which showed the exact same oscillations with current balancing being disabled. It is noted that the ripple appearing in the waveforms of Figs. 6(b, d) is due to the existence of current imbalance.

Finally, as another example of transient condition, Fig. 7 illustrates the starting behaviour of the same motor, with the proposed method being enabled in Fig. 7(a) and disabled in Fig. 7(b). It can be seen that, neglecting the high-frequency ripple of Fig. 7(b), the system response is similar in both cases. Thus, a motor can be started with the proposed method enabled. Alternatively, the method can be enabled when the starting procedure is complete, since there is normally negligible effect if current imbalance appears only for the few seconds of the starting process.

4. Experimental results

The proposed algorithm was tested experimentally on an induction motor (ABB model M20A200L6A), driven by a 480V-260kVA VSD designed for ESP applications, through a step-up transformer and a long ESP flat armored cable. A block diagram of the experimental setup is presented in Fig. 8. The VSD is equipped with a sine filter, which

is a requirement for applications with long motor cables [6], while the step-up transformer was included in the setup to replicate an actual ESP installation. Photographs of the VSD, cable, transformer and motor are shown in Fig. 9, while their main parameters are listed in Tables 3 and 4. The VSD was an Electrospeed Advantage™ by Baker Hughes, with a modified controller board and HMI. The motor controller used the structure of Fig. 2 and was implemented in an Intel Cyclone FPGA. The *k* gain for the SOGIs was set to 1, and the negative-sequence current PI controllers' proportional gain and integral time constant were set to 0.5 (V/A) and 30 ms, respectively.

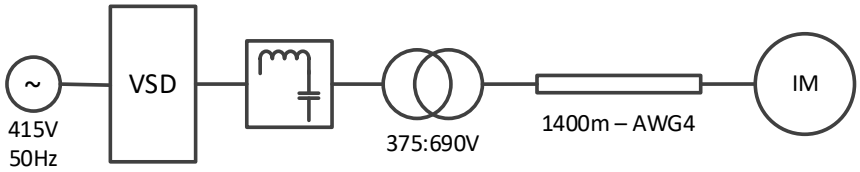

Fig. 8. Block diagram of the experimental setup.

(a) (b)

Fig. 9. Photographs of (a) VSD, and (b) cable, transformer and motor of the experimental setup.

Table 3. Cable parameters.

Parameter	Value
Type	Flat, armored
Size	AWG 4
Length	1400 m
Resistance at 25 °C	1.17 Ω

Table 4. Motor nameplate parameters.

Parameter	Value
Rated voltage	440 V
Rated current	36.6 A
Rated frequency	60 Hz
Rated speed	1175 rpm
Power factor (cosφ)	0.84

Fig. 10 illustrates the effect of enabling the proposed current balancing method on the waveforms of the three drive output currents, while running with two different electrical frequencies: 45 Hz and 60 Hz. In Figs. 10(a, c) the three currents are heavily imbalanced, while in Figs. 10(b, d), the imbalance is suppressed. The same effect is manifested through the corresponding current RMS values, listed in Table 5. The three currents initially have unequal RMS values, resulting in a current imbalance of 9.2%. After enabling the proposed method, the three RMS values become approximately equal, with the imbalance reducing to 1%. The maximum remaining difference between the three RMS currents is 0.3 A, which is in the range of the VSD's current sensor accuracy and measurement circuit's resolution.

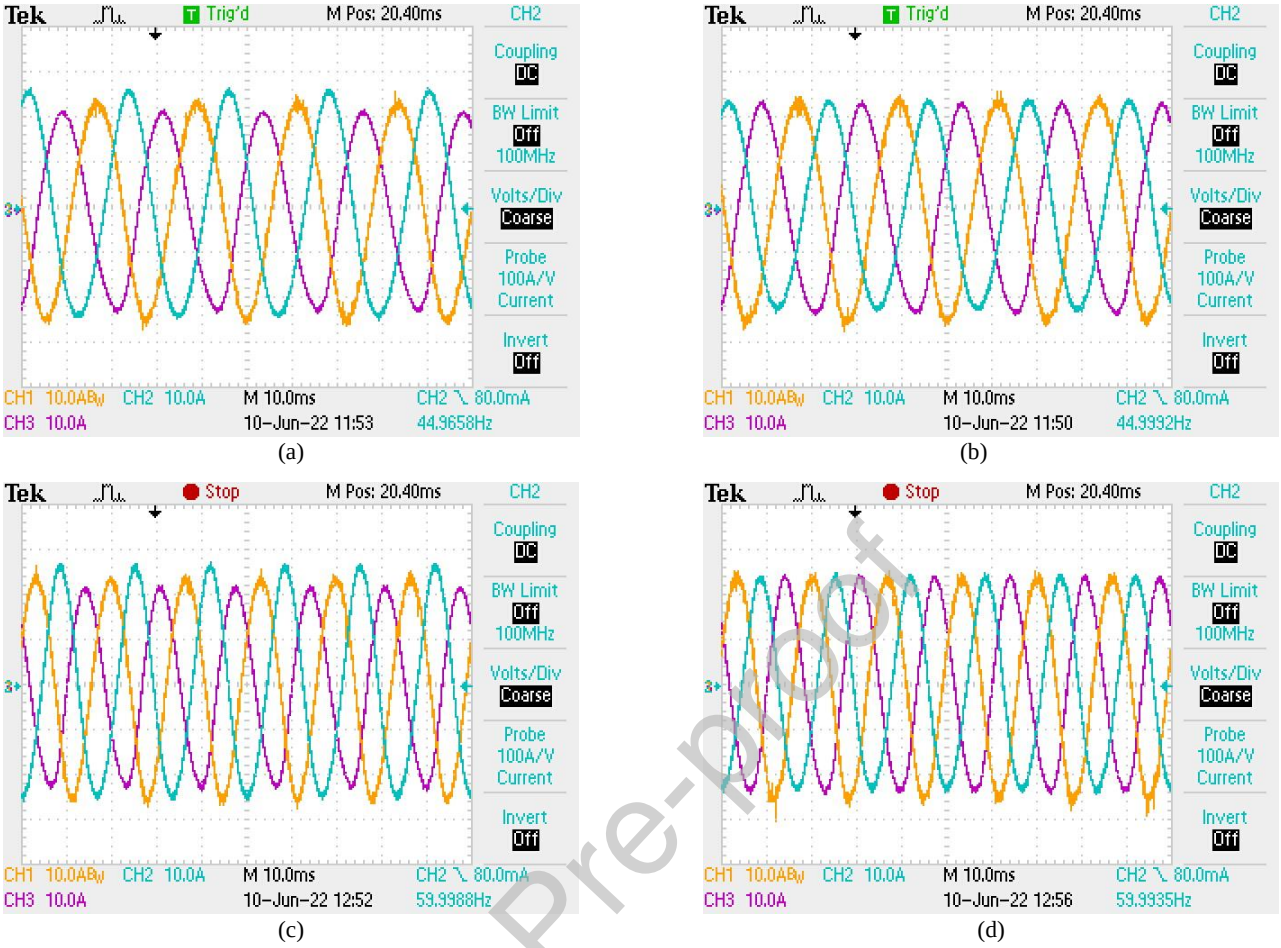

Fig. 10. Oscilloscope shots illustrating the three drive output currents while running with an electrical frequency of 45 Hz (a, b) and 60 Hz (c, d), before (a, c), and after (b, d) enabling the proposed current balancing method.

Table 5. RMS values of output currents and line voltages with current balancing disabled/enabled.

Parameter	Current balancing disabled	Current balancing enabled
Phase current I_A (A)	16.2	16.7
Phase current I_B (A)	18.2	16.5
Phase current I_C (A)	15.6	16.8
Line voltage V_{AB} (V)	150	149
Line voltage V_{BC} (V)	150	152
Line voltage V_{CA} (V)	150	151
Current imbalance (%)	9.2	1

Furthermore, it can be observed in Table 5 that the three drive output voltages become slightly imbalanced, which is due to the addition of the negative-sequence reference voltages ($u_{abc,-}$ in Fig. 2) to the balanced reference voltages of the original scalar algorithm ($u_{abc,sc}$ in Fig. 2). The voltage imbalance is negligible (around 1%) and has no effect on the drive operation but is still adequate to correct the significant initial current imbalance. Finally, Fig. 11 presents internal data of the current balancing algorithm before and after enabling it, while running at the frequency of 60 Hz. The figure illustrates the output currents as seen by the drive and the negative-sequence currents calculated as part of the proposed method. These results further validate the effectiveness of the proposed method.

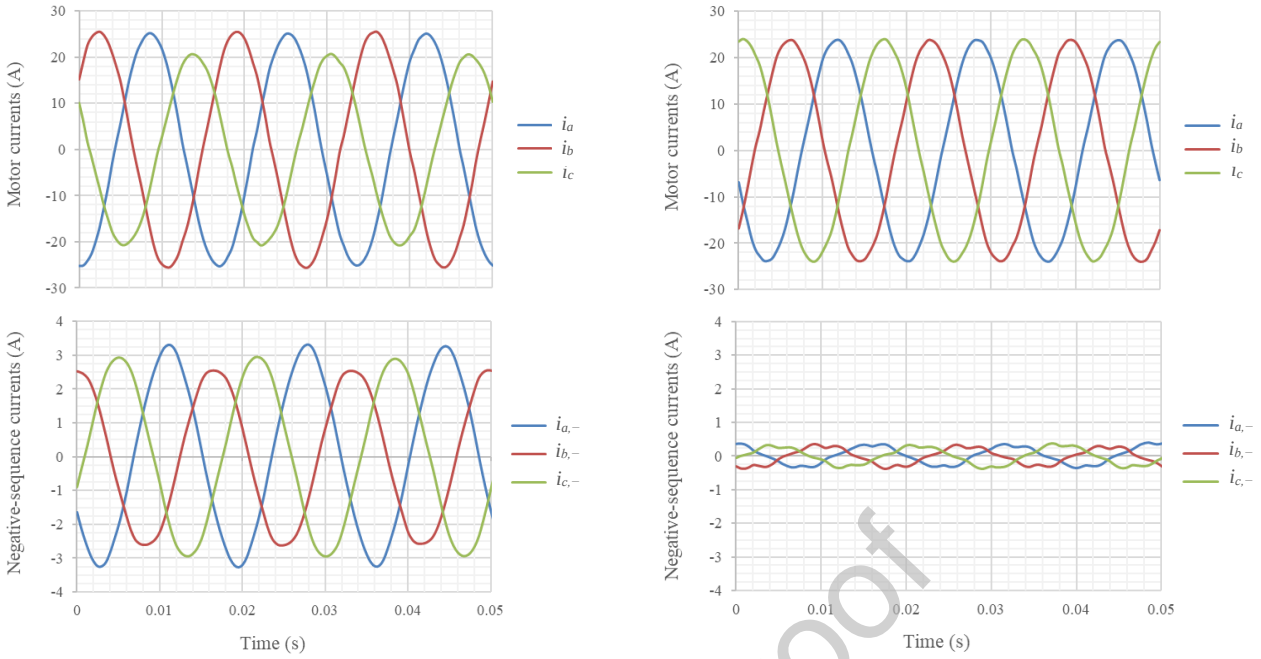

Fig. 11. Internal data of the current balancing algorithm (a) before, and (b) after enabling it, while running at 60 Hz.

5. Discussion

This section discusses certain limitations of the proposed method and provides guidelines for practical implementations and suggestions for future work.

5.1. Limitations

The following limitations have been identified with regards to the proposed current balancing method:

- The method may not be as effective when the current imbalance is very small compared to the rated drive current. This is because the resolution of the output current sensors and the respective ADCs may not be high enough to distinguish small differences among the output currents, or the ADC's calibration may not be adequately accurate. An example outcome can be observed in Figures 9(b) and 9(d), where the three currents are not exactly balanced; they still have a 1% imbalance, as also reported in Table 5. Moreover, the three-phase currents shown in the top graphs of Fig. 11 do not exactly match the respective ones shown in Figs. 10(c) and 10(d), while the negative-sequence currents in the bottom graph of Fig. 11(a) do not have the typical form of a balanced three-phase set (according to the theory of symmetrical components). The reason for the above is that the drive used in the experiments had a rated current of 313 A, whereas the experiments were performed with current of approximately 17 A (on average between the three phases), which corresponds to 5.43% of the drive rating.
- The proposed method slightly increases the peak value of the drive reference voltages, which is due to the injection of a negative-sequence component into them. Although this component is normally negligible as compared to the positive-sequence voltage component (as shown in Figure 5 and Table 5), it may lead to over-modulation when the inverter is already operating at the limit of its linear region (i.e., with a modulation index of 100%).
- The proposed method can effectively suppress current unbalance under steady-state operating conditions using moderate gains for its negative-sequence PI controllers, which are lower than those suggested by

conventional tuning methods [38]. Lower gains can be preferable to avoid intense variations to the voltage references, which could cause over-modulation or resonance in VSDs with sine filters. On the other hand, reducing the controller gains may not suppress small-scale imbalances that can appear during transients. These imbalances are normally acceptable in artificial lift and other applications where the motor mostly runs at constant speed and torque, since they last for short time intervals and thus do not practically affect the motor and driven equipment. However, they may need to be suppressed by adopting higher gains in applications which involve frequent and intense torque/speed variations.

5.2. Relation with the scalar-controlled induction motor instability effect

The stability of a scalar-controlled induction motor drive is a known issue that has been studied extensively in the literature. Instability exhibited as sustained oscillations is often experienced in cases when the driven equipment has low inertia and low damping. It is also known to be affected by machine and drive parameters including stator resistance, dead time, dc-link capacitance and system resonance frequencies. Several methods have been proposed to prevent the instability, such as those presented in references [41 – 45]. These methods modify the conventional *V/f* algorithm voltage references by injecting into them compensating signals, typically calculated in the synchronous (d-q) reference frame. In all cases, the stabilizing methods act on the positive-sequence voltage generation, since the angle used for the respective transformations varies in accordance with the sign of the algorithm frequency.

The above literature does not include negative-sequence voltages/currents among the factors affecting the instability, and the stabilizing methods do not act on them. This suggests that the proposed current balancing method is likely to not affect it, either, but further research is required to confirm that. In any case, the proposed method could be executed in combination with a stabilizing method, since the latter acts only on the positive-sequence voltages. Decoupling of the positive- from the negative-sequence currents may be required in this case (e.g., by filtering the double-fundamental frequency components in d-q coordinates) in the stabilizing method. With reference to artificial lift applications, it is also worth noting that ESP pumps have a quadratic torque-speed characteristic, which provides high damping and enhances stability.

The comparative simulations in transient conditions (torque step and frequency variation) shown in Figs. 6(a) – (d) support the above argument. The oscillations appearing in these figures relate to the instability effect. The oscillations are decaying in these cases, i.e., the instability is not sustained, but their characteristics demonstrate that the current balancing method has no effect on them. Namely, it can be observed that the system response (drive output currents, electromagnetic torque, angle difference, angular frequency difference) is similar with the method enabled (a, c) and disabled (b, d), apart from the ripple appearing in the latter due to the existence of current imbalance. The comparative simulations referring to motor starting, whose results were presented in Fig. 7, also show the same effect.

5.3. Suggestions for practical implementations and future work

Based on the above discussion, the following guidelines can be provided for practical implementations and future work on the proposed method:

- In order to maximize the effect of the proposed algorithm, accurate current sensors must be selected, and careful calibration must be performed.
- Further research is required to confirm that the proposed method does not affect the stability of *V/f*-driven induction motors.
- Further control analysis will be required to optimally tune the proposed controller for high performance under challenging operating conditions, such as highly variable speed/load.

6. Conclusion

This paper presented a control method for mitigating current imbalance that appears in scalar-controlled IMs driven through long imbalanced power cables. The method does not require hardware additions/modifications and does not

depend on the knowledge of cable parameters, which is required for the implementation of other alternatives. It is straightforward to implement as an extension to existing scalar control algorithms, since it makes use of internal scalar algorithm variables. Moreover, it eliminates the need for implementing an imbalance-immune flux observer, thus offering increased robustness and significant saving in computational resources. The simulation and experimental results included in the paper demonstrate its effectiveness in a variety of steady-state and dynamic operating conditions, while limitations, implementation details and future work are also discussed. The proposed method is of particular significance for artificial lift applications, where it offers a practical solution to well-known problems induced from current imbalance, avoiding several downsides of existing current balancing approaches.

Acknowledgements

Funding: This work was supported by TSL Technology Ltd, Ropley, UK.

References

[1] G. I. Orfanoudakis, M. A. Yuratich and S. M. Sharkh, "Current balancing of scalar-controlled induction motors with imbalanced cables," *14th Seminar on Power Electronics and Control (SEPOC)*, Santa Maria, Brazil, 2022, pp. 1-6.

[2] J. M. Tabora, M. E. De Lima Tostes, E. O. De Matos, U. H. Bezerra, T. M. Soares and B. S. De Albuquerque, "Assessing Voltage Unbalance Conditions in IE2, IE3 and IE4 Classes Induction Motors, " *IEEE Access*, vol. 8, pp. 186725-186739, 2020.

[3] A. von Jouanne and B. Banerjee, "Assessment of voltage unbalance," *IEEE Transactions on Power Delivery*, vol. 16, no. 4, pp. 782-790, Oct. 2001.

[4] T. R. Brinner, "Voltage and Cable Impedance Unbalance in Submergible Oil Well Pumps," *IEEE Transactions on Industry Applications*, vol. IA-20, no. 1, pp. 97-104, Jan. 1984.

[5] J. Timmerberg and S. Mylvaganam, "Inductance of 3-phase transmission lines of different layouts with focus on cables in flat formation," *12th IEEE International Symposium on Electronics and Telecommunications (ISETC)*, Timisoara, Romania, 2016, pp. 235-238.

[6] A. J. Williams and D. Shipp, "ESP Downhole Power Quality - Do We have a Healthy Cardiovascular System?" *SPE Gulf Coast Section Electric Submersible Pumps Symposium*, The Woodlands, Texas, USA, May 2019.

[7] J. E. Layton, "Three phase flat cable inductance balancer," US patent 6,566,769 B1, 2003.

[8] M. A. Zagrodnik, "A three-phase AC electrical system and a method for compensating an inductance imbalance in such a system," International Patent WO 2014/086363 A2, 2014.

[9] M. L. Crane, S. Kremeier, and R. Mc-Coy, "Systems and methods for balancing unbalanced power cables," International Patent WO 2021/097099 A1, 2021.

[10] M. Reyes, P. Rodriguez, S. Vazquez, A. Luna, R. Teodorescu and J. M. Carrasco, "Enhanced Decoupled Double Synchronous Reference Frame Current Controller for Unbalanced Grid-Voltage Conditions," *IEEE Transactions on Power Electronics*, vol. 27, no. 9, pp. 3934-3943, Sept. 2012.

[11] Y. Yu, Z. Wang, and X. Wan, "Optimal Current Balance Control of Three-Level Inverter under Grid Voltage Unbalance: An Adaptive Dynamic Programming Approach," *Energies*, vol. 12, no. 15, p. 2864, Jul. 2019.

[12] S. B. Q. Naqvi and B. Singh, "Weak Distribution Grid Interfaced PV-Battery System With Modified Second Order Sequence Filter Based Control Strategy and Grid Supportive Features," in *IEEE Transactions on Industry Applications*, vol. 59, no. 2, pp. 2352-2362, March-April 2023.

[13] G. I. Orfanoudakis, S. M. Sharkh and M. A. Yuratich, "Combined Positive-Sequence Flux Estimation and Current Balancing for Sensorless Motor Control Under Imbalanced Conditions," *IEEE Transactions on Industry Applications*, vol. 57, no. 5, pp. 5099-5107, Sept.-Oct. 2021.

[14] Y. Hu, Z. -Q. Zhu and K. Liu, "Current Control for Dual Three-Phase Permanent Magnet Synchronous Motors Accounting for Current Unbalance and Harmonics," in *IEEE Journal of Emerging and Selected Topics in Power Electronics*, vol. 2, no. 2, pp. 272-284, June 2014.

[15] L. Zhu, L. Wu, J. Liu and Y. Guo, "Negative Sequence Current Suppression of Dual Three-Phase Permanent Magnet Synchronous Machines Considering Inductance Asymmetry," *2019 22nd International Conference on Electrical Machines and Systems (ICEMS)*, Harbin, China, 2019, pp. 1-6.

[16] M. Mengoni, L. Zarri, Y. Gritli, A. Tani, F. Filippetti and S. B. Lee, "Online Detection of High-Resistance Connections With Negative-Sequence Regulators in Three-Phase Induction Motor Drives," in *IEEE Transactions on Industry Applications*, vol. 51, no. 2, pp. 1579-1586, March-April 2015.

[17] H. Gu, Z. Cai, Z. Wang, Y. Zhang, W. Dong and R. Guo, "Three-Phase Current Unbalance Suppression Method of Linear Induction Motor Based on PR Controller," *2022 4th International Conference on Smart Power & Internet Energy Systems (SPIES)*, Beijing, China, 2022, pp. 883-888.

[18] P. Rodríguez, R. Teodorescu, I. Candela, A. V. Timbus, M. Liserre and F. Blaabjerg, "New positive-sequence voltage detector for grid synchronization of power converters under faulty grid conditions," *37th IEEE Power Electronics Specialists Conference*, 2006, pp. 1-7.

[19] P. Rodriguez, A. Luna, M. Ciobotaru, R. Teodorescu and F. Blaabjerg, "Advanced Grid Synchronization System for Power Converters under Unbalanced and Distorted Operating Conditions," *32nd Annual Conference on IEEE Industrial Electronics (IECON)*, Paris, 2006, pp. 5173-5178.

[20] P. Rodriguez, A. Luna, I. Candela, R. Mujal, R. Teodorescu and F. Blaabjerg, "Multiresonant Frequency-Locked Loop for Grid Synchronization of Power Converters Under Distorted Grid Conditions," *IEEE Transactions on Industrial Electronics*, vol. 58, no. 1, pp. 127-138, Jan. 2011.

[21] M. Ciobotaru, R. Teodorescu, F. Blaabjerg, "A new single phase PLL structure based on second order generalized integrator," *IEEE Power Electronics Specialists Conference*, pp. 1-6, 2006.

[22] A. Bamigbade and V. Khadkikar, "Extended State-Based OSG Configurations for SOGI PLL With an Enhanced Disturbance Rejection Capability," in *IEEE Transactions on Industry Applications*, vol. 58, no. 6, pp. 7792-7804, Nov.-Dec. 2022.

[23] S. Mohamadian, H. Pairo and A. Ghasemian, "A Straightforward Quadrature Signal Generator for Single-Phase SOGI-PLL With Low Susceptibility to Grid Harmonics," in *IEEE Transactions on Industrial Electronics*, vol. 69, no. 7, pp. 6997-7007, July 2022.

[24] G. Modi and B. Singh, "Improved Cascaded SOGI Control for Islanding-Synchronization in Photovoltaic System," in *IEEE Transactions on Industry Applications*, vol. 58, no. 6, pp. 6909-6919, Nov.-Dec. 2022.

[25] W. Shi, J. Yu and R. Zhou, "A Zero-Tracking SOGI-Based Frequency-Locked Loop," in *IEEE Journal of Emerging and Selected Topics in Power Electronics*, vol. 10, no. 3, pp. 3114-3128, June 2022.

[26] J. Xu, H. Qian, Q. Qian and S. Xie, "Modeling, Stability, and Design of the Single-Phase SOGI-Based Phase-Locked Loop Considering the Frequency Feedback Loop Effect," in *IEEE Transactions on Power Electronics*, vol. 38, no. 1, pp. 987-1002, Jan. 2023.

[27] S. Prakash, J. K. Singh, R. K. Behera and A. Mondal, "A Type-3 Modified SOGI-PLL With Grid Disturbance Rejection Capability for Single-Phase Grid-Tied Converters," in *IEEE Transactions on Industry Applications*, vol. 57, no. 4, pp. 4242-4252, July-Aug. 2021.

[28] G. Orfanoudakis and M. Yuratich, "SOGI-based integrator, PLL and current controller for grid connection and motor control," International Patent WO 2018/157120 A1, 2018.

[29] G. I. Orfanoudakis, S. M. Sharkh and M. A. Yuratich, "Positive-sequence flux estimator based on Second-Order Generalized Integrators for grid synchronization and motor control under imbalanced conditions," *21st European Conference on Power Electronics and Applications (EPE)*, 2019, pp. 1-10.

[30] G. Wang et al., "Enhanced Position Observer Using Second-Order Generalized Integrator for Sensorless Interior Permanent Magnet Synchronous Motor Drives," *IEEE Transactions on Energy Conversion*, vol. 29, no. 2, pp. 486-495, June 2014.

[31] Y. Jiang, W. Xu and C. Mu, "Improved SOIFO-based rotor flux observer for PMSM sensorless control," *43rd Annual Conference of the IEEE Industrial Electronics Society (IECON)*, Beijing, 2017, pp. 8219-8224.

[32] B. Liu, B. Zhou and T. Ni, "Principle and Stability Analysis of an Improved Self-Sensing Control Strategy for Surface-Mounted PMSM Drives Using Second-Order Generalized Integrators," *IEEE Transactions on Energy Conversion*, vol. 33, no. 1, pp. 126-136, Mar. 2018.

[33] I. Ralev, A. Klein-Hessling, B. Pariti and R. W. De Doncker, "Adopting a SOGI filter for flux-linkage based rotor position sensing of switched reluctance machines," *IEEE International Electric Machines and Drives Conference (IEMDC)*, Miami, FL, 2017, pp. 1-7.

[34] R. Zhao, Z. Xin, P. C. Loh and F. Blaabjerg, "A novel flux estimator based on SOGI with FLL for induction machine drives," *IEEE Applied Power Electronics Conference and Exposition (APEC)*, Long Beach, CA, 2016, pp. 1995-2002.

[35] Z. Xin, R. Zhao, F. Blaabjerg, L. Zhang and P. C. Loh, "An Improved Flux Observer for Field-Oriented Control of Induction Motors Based on Dual Second-Order Generalized Integrator Frequency-Locked Loop," *IEEE Journal of Emerging and Selected Topics in Power Electronics*, vol. 5, no. 1, pp. 513-525, Mar. 2017.

[36] R. Zhao, Z. Xin, P. C. Loh and F. Blaabjerg, "A Novel Flux Estimator Based on Multiple Second-Order Generalized Integrators and Frequency-Locked Loop for Induction Motor Drives," *IEEE Transactions on Power Electronics*, vol. 32, no. 8, pp. 6286-6296, Aug. 2017.

[37] M. Kashif, S. Murshid and B. Singh, "Solar PV Array Fed Self-Sensing Control of PMSM Drive With Robust Adaptive Hybrid SOGI Based Flux Observer for Water Pumping," in *IEEE Transactions on Industrial Electronics*, vol. 68, no. 8, pp. 6962-6972, Aug. 2021.

[38] Liuping Wang; Shan Chai; Dae Yoo; Lu Gan; Ki Ng, "PID Control System Design for Electrical Drives and Power Converters," in *PID and Predictive Control of Electrical Drives and Power Converters using MATLAB / Simulink* , IEEE, 2015, pp.41-85.

[39] S. Chapman. *Electric Machinery Fundamentals*, 5th ed., New York, N.Y.: McGraw-Hill, 2012.

[40] P. Pillay and M. Manyage, "Definitions of Voltage Unbalance," *IEEE Power Engineering Review*, vol. 21, no. 5, pp. 49-51, May 2001.

[41] G.-J. Jo and J.-W. Choi, "Rotor Field-Oriented V/f Drive System Implementation With Oscillation Suppression Compensator in Induction Motors," in *IEEE Journal of Emerging and Selected Topics in Power Electronics*, vol. 9, no. 3, pp. 2745-2758, June 2021.

[42] L. Tiitinen, M. Hinkkanen and L. Harnefors, "Stable and Passive Observer-Based V/Hz Control for Induction Motors," *2022 IEEE Energy Conversion Congress and Exposition (ECCE)*, Detroit, MI, USA, 2022, pp. 1-8.

[43] B. Chen, W. Yao, Z. Lu and K. Lee, "A novel stator flux oriented V/f control method in sensorless induction motor drives for accuracy improvement and oscillation suppression," *2014 IEEE Energy Conversion Congress and Exposition (ECCE)*, Pittsburgh, PA, USA, 2014, pp. 5092-5099.

[44] K. Suzuki, S. Saito, T. Kudor, A. Tanaka and Y. Andoh, "Stability Improvement of V/F Controlled Large Capacity Voltage-Source Inverter Fed Induction Motor," *Conference Record of the 2006 IEEE Industry Applications Conference Forty-First IAS Annual Meeting*, Tampa, FL, USA, 2006, pp. 90-95.

[45] A. A. Popa, A. Isfanuti, L. Tutelea and I. Boldea, "V/f with stabilizing loops fast response control of Induction Motor (IM) drives," *2021 International Aegean Conference on Electrical Machines and Power Electronics (ACEMP) & 2021 International Conference on Optimization of Electrical and Electronic Equipment (OPTIM)*, Brasov, Romania, 2021.

Author Biography

Georgios I. Orfanoudakis (M'14) received his MEng in electrical engineering and computer science from the National Technical University of Athens (NTUA), Greece, in 2007, and his PhD on power electronic converters from the University of Southampton, UK, in 2013.

From 2012 until 2019 he worked with the University of Southampton as a Research Associate (2012-2014), the Hellenic Mediterranean University as a Teaching Fellow (2014-2019) and with TSL Technology Ltd, as a Power Electronics R&D Engineer. In 2020 he was appointed by the Electrical and Computer Engineering department of the Hellenic Mediterranean University, Crete, Greece, as an Assistant Professor of Power Electronics and Motor Drives. His research focuses on topologies and modulation strategies of multilevel and PV inverters, and on sensorless control of motor drives.

Suleiman M. Sharkh is Professor of Power Electronics, Machines and Drives in the Faculty of Engineering and the Physical Sciences at the University of Southampton. He the Deputy Director of the Southampton EPSRC Energy Storage and its Applications Centre for Doctoral Training and was past Head of the Mechatronics Research Group.

He has over 20 years research experience in electric machines, power electronics and their applications in transport, renewable energy and microgrids. He has published over 160 papers, supervised over 20 PhD students to completion.

Prof Sharkh was the winner of The Engineer Energy Innovation and Technology Award 2008 for his work on novel rim driven marine thrusters and turbine generators. He is a Senior Member of the IEEE, a member of the IET and a Chartered Engineer.

Michael A. Yuratich is Managing Director of TSL Technology Limited and co-founder of Magnetic Pumping Solutions LLC. He received his BSc(Hons) in Electronics Science in 1974 and his PhD in Nonlinear Optics in 1977, subsequently becoming Ramsay Memorial Fellow and lecturer in Electronics, all at the University of Southampton. At the University of Southampton, he also contributed to the Industrial Mathematics MSc course and is a Visiting Scholar.

In his industrial career he has worked widely in electro-mechanical systems and instrumentation for downhole exploration equipment. He holds 65 patents and has published 20 papers and a book.

Dr Yuratich was the winner of The Engineer Energy Innovation and Technology Award 2008 for integrated thrusters, and twice winner of Society of Petroleum Engineer technology awards. He is a Chartered Physicist.

Declaration of Interests

☒ The authors declare that they have no known competing financial interests or personal relationships that could have appeared to influence the work reported in this paper.

☐ The authors declare the following financial interests/personal relationships which may be considered as potential competing interests: